Isoelectric point determination by icIEF as quality control for structural and functional characterization of HPV16 virus-like particles

Aurore Boclinville[1], Marylène Vandevenne[2], Anne Pressia[1], Nicolas Thelen[3], Marc Thiry[3], Nathalie Jacobs[4], Alain Brans[2], Marianne Fillet[1], Anne-Catherine Servais[1]

[1]Laboratory for the Analysis of Medicines (LAM), Center for Interdisciplinary Research on Medicines (CIRM), University of Liège, Liège, Belgium; [2]InBioS - Centre for Protein Engineering, Département des Sciences de la Vie, University of Liège, Liège, Belgium; [3]Cellular and Tissular Biology, GIGA-Neurosciences, University of Liège, Liège, Belgium; [4]Cellular and Molecular Immunology, GIGA-Research, University of Liège, Liège, Belgium

***Corresponding author:** Prof. Anne-Catherine Servais, Laboratory for the Analysis of Medicines (LAM), CIRM, University of Liège, Quartier Hôpital, B36, Avenue Hippocrate 15, B-4000 Liège, Belgium

E-mail address: acservais@uliege.be

Abstract

Background: Human papillomavirus virus-like particles (HPV-VLPs) are widely used as vaccine antigens and research models due to their structural similarity to native virions. Their production relies on the use of an expression system and involves complex molecular and biochemical steps. Slight variations in these steps can lead to batch-to-batch differences. However, process consistency and conformational integrity are critical to ensure their biological functionality. There is a great need for a tool to assess the structural integrity and batch consistency of HPV16-VLPs.

Results: In this study, we developed and validated a robust imaged capillary isoelectric focusing (icIEF) method to assess the isoelectric point (pI) of intact HPV16-VLPs as a sensitive quality control (QC) metric. Key method parameters, namely surfactant and urea content, together with focusing time were optimized to maintain VLP stability during icIEF analysis. The method was validated according to ICH Q2(R2) guidelines and demonstrated high specificity, precision, and accuracy. Analysis of multiple production batches revealed two distinct VLP populations with pIs around 6.4 and 7.5, respectively. While conventional QC tests could not discriminate between these batches, functional assays (performed using bio-layer interferometry and affinity capillary electrophoresis) showed an altered binding capacity to laminin 332 receptor for the high pI VLPs. A disassembly/reassembly process restored the lower pI and binding capacity, suggesting conformational differences as the underlying cause.

Significance: This work highlights icIEF as a powerful orthogonal tool capable of detecting subtle structural and functional changes in complex biotherapeutics. It supports the implementation of this method into routine QC strategies to enhance both the reliability of research outcomes and the safety and efficacy of VLP-based vaccines.

Keywords

Human papillomavirus, virus-like particles, vaccine, isoelectric point, characterization, imaged capillary isoelectric focusing

Abbreviations

ACE, affinity capillary electrophoresis; BGE, background electrolyte; BLI, bio-layer interferometry; HPV, human papillomavirus; icIEF, imaged capillary isoelectric focusing; K_D, equilibrium dissociation constant; k_{off}, dissociation rate constant; k_{on}, association rate constant; LN, laminin; M, internal marker; MC, methylcellulose; pI, isoelectric point; QC, quality control; TEM, transmission electron microscopy; VLP, virus-like particle.

1. Introduction

Human papillomavirus (HPV) is a non-enveloped, double-stranded DNA virus that infects epithelial cells and causes diseases ranging from benign lesions to invasive cancers, particularly in the anogenital and oropharyngeal regions [1, 2]. More than 400 HPV types have been identified and are classified into low- and high-risk groups. Amond these, HPV16 and HPV18 are responsible for 70 % of cervical cancers [2-5].

HPV capsid is composed of two structural proteins, L1 and L2. The major capsid protein L1 is approximately 55 kDa and self-assembles into a stable, icosahedral structure with 360 copies organized into 72 pentamers in a $T = 7$ lattice [2, 6, 7]. The role of the minor capsid protein, L2, includes providing structural support and aiding infection, with up to 72 copies per capsid [8, 9]. Due to the complexity of HPV culture *in vitro*, HPV virus-like particles (VLPs) composed of L1 or both L1 and L2 proteins are often used in research. These VLPs, that exhibit a diameter of about 55 nm, are morphologically and immunologically similar to native HPV, making them essential in HPV studies and in vaccines development [10]. HPV-VLPs L1 are the basis for the vaccines Cervarix® and Gardasil®9, which are highly effective in preventing infections from HPV types linked to cancer and to genital warts. The high structural fidelity and non-infectious nature of VLPs make them an asset for both research and therapeutic applications in virology and immunology.

In order to obtain consistent and reliable research results, it is essential to ensure the quality, purity, and functionality of experimental reagents, particularly biological reagents produced using expression systems [11, 12]. The production of biologics involves complex molecular and biochemical steps, and slight variations in these steps can lead to batch-to-batch differences. Therefore, quality control (QC) tests to assess the identity, the purity, the content as well as the stability of biologics have to be carried out before their use in downstream experiments, whatever their source, i.e. if they are obtained from commercial suppliers or produced by the researchers themselves. Biologics cover different types of substances with increasing complexity, such as peptides, proteins, antibodies and VLPs, the latter requiring additional QC tests to establish their morphology, size and their surface properties [13].

A promising technique for enhanced QC of VLPs is imaged capillary isoelectric focusing (icIEF). This technique separates the analytes based on their isoelectric points (pI), the pH at which their net charge is equal to zero. It has demonstrated utility in the QC of biologics, and more particularly in monoclonal antibody characterization, where pI variations can indicate changes in protein folding, post-translational modifications, or aggregation states that may influence functionality [14, 15]. An icIEF method was developed by Chao-Ming Zhou to characterize the L1 proteins of HPV18 and HPV16 [16]. However, it remains unclear if the determined pI values correspond to the L1 proteins or to the intact HPV-VLPs. Other studies have explored the use of icIEF for analyzing intact viruses or VLPs, highlighting the potential of this technique for resolving charge heterogeneity in large macromolecular assemblies. These include work on norovirus VLPs, where icIEF enabled determination of isoelectric points and differentiation of particle populations [17, 18]; hepatitis E VLPs, where charge variants were characterized [19]; bacteriophage MS2, where differences between intact virions, disrupted particles, and virus-antibody complexes were resolved [20] and poliovirus, where different types were characterized [21]. These findings demonstrate that icIEF can be adapted for the analysis of intact viral structures when optimized appropriately. Applying icIEF to HPV-VLPs requires careful optimization to preserve particle integrity during analysis. Because VLPs are complex, self-assembled structures, maintaining the stability of their intact form throughout the icIEF process is essential. In this study, parameters such as surfactant addition, urea concentration and focusing time were evaluated to ensure that the VLPs do not disassemble or aggregate under analysis conditions. This guarantees that icIEF analysis captures characteristics of the VLPs in their functional form, thus providing a comprehensive assessment of their structural and functional integrity.

After validation according to ICH Q2(R2) guidelines, the icIEF method was applied to investigate the variability of the pI value of HPV16-VLPs among various batches. Differences in pI were correlated with variations in functional properties, which were further linked to conformational differences. These findings demonstrate the potential of icIEF not only as a powerful QC tool to monitor batch-to-batch consistency of complex biologics, but also to detect subtle structural changes that may impact product functionality, such as changes that are not always captured by conventional quality control methods. A control chart was established to facilitate ongoing monitoring of such critical quality attributes.

2. Materials and methods

2.1. Chemicals and reagents

Tris(hydroxymethyl)aminomethane hydrochloride (Tris HCl), poly(ethylene oxide) (PEO) (MW 200,000 g mol^{-1}), 2-[4-(2-hydroxyethyl)-1-piperazinyl]-ethane-sulfonic acid sodium salt (HEPES-Na), sodium citrate, phthalic acid, urea, polysorbate 80 (Tween® 80), dithiothreitol (DTT), and bovine serum albumin (BSA) were obtained from Sigma-Aldrich (Saint-Louis, United-States). Hydrochloric acid fuming 37 % w/w (HCl), ortho-phosphoric acid 85 % w/w (H_3PO_4), sodium chloride (NaCl), polyethylene glycol (PEG) 6000, and glycine were provided by Merck (Darmstadt, Germany). Sodium hydroxide (NaOH), disodium hydrogen phosphate, sulfuric acid 95-98 % w/w and polysorbate 20 (Tween® 20) were purchased from VWR (Leuven, Belgium). Sodium dodecyl sulfate (SDS) was obtained from Fisher Scientific (Loughborough, United Kingdom). Ethylenediaminetetraacetic acid (EDTA) was acquired from Acros Organics (New Jersey, USA). Laminin 332 (LN332) 0.1 mg mL^{-1} was sourced by Bio-Connect (Huissen, The Netherlands). Phosphate buffered saline (PBS) was provided by Lonza (Bâle, Switzerland). 96-well plates Nunc Maxisorp were obtained from Thermo Fisher Scientific (Waltham, USA). CEInfinite Super High resolution AESlyte pH 3-10, CEInfinite methylcellulose (MC) 1 % w/w, CEInfinite isoelectric point markers 4.14, 5.12, 6.61 and 9.22, CEInfinite anolyte and CEInfinite catholyte were purchased from ISOGEN Life Science (De Meern, Pays-Bas). Rabbit anti-mouse HRP antibody was obtained from Dako (Glostrup, Denmark). HPV16 L1 conformational antibody supernatant was kindly provided by Pr. M. Müller (German Cancer Research Center (DKFZ), Heidelberg, Germany). Gardasil®9 (HPV-VLP based vaccine) from Merck & Co. (Lyon, France) was also used. Ultra-pure water was supplied by a Milli-Q equipment (Millipore, Bedford, MA, USA) and Chromafil® Xtra PVDF syringe filters (0.20 µm) were from Macherey-Nagel (Düren, Germany).

2.2. HPV-VLP samples

HPV16-VLPs were produced using the baculovirus-insect cells expression system. SF21 insect cells (kindly provided by Pr. A. Touzé, UMR INRAE ISP, Université de Tours, Tours, France) were infected by a recombinant baculovirus carrying L1 gene of HPV16, kindly provided by Pr. M. Müller. These cells were then harvested and HPV16-VLPs were purified on a cesium chloride gradient following the procedure described in [10]. HPV16-VLPs were finally resuspended in 150 mM NaCl and 0.01 % v/v Tween® 80. L1 protein was quantified using a micro-BCA protein assay kit obtained from Thermo Fisher Scientific (Waltham, USA).

2.3. HPV-VLP sample quality control

HPV16-VLP samples were characterized using different techniques. HPV16-VLP morphology and size were checked by transmission electron microscope (TEM) (cf. Supplementary Fig. S1). For this purpose, HPV16-VLPs were applied on a carbon film grid (Laborimpex, Brussel, Belgium) for 2 min and negatively stained with 1.5 % w/v ethanolic uranyl acetate for 2 min. Observations were carried out on a JEM-1400 transmission electron microscope (JEOL Ltd., Tokyo, Japan) operating at an accelerating voltage of 80 kV. For the identification and assay of HPV16-VLPs, an ELISA was performed with a conformational antibody following the protocol described by Bettonville et al. [22]. The antigenic purity was evaluated by SDS-PAGE. Nupage® Bis-Tris gel 10 % and SeeBlue Plus 2 Prestained Protein ladder, used as molecular weight markers, provided by Thermo Fisher Scientific (Waltham, USA) were used. The electrophoretic profiles were revealed by SYPRO® ruby protein gel stain purchased from Thermo Fisher Scientific (Waltham, USA).

2.4. icIEF experiments

2.4.1. Instrumentation

Experiments were performed using a preparative CEInfinite system and WCID cartridges (100 µm id) with fluorocarbon coating from Advanced Electrophoresis Solutions Ltd. (AES) (Cambridge, ON, Canada) equipped with an autosampler and an on-column UV detection at 280 nm.

2.4.2. Isoelectric focusing conditions

For icIEF separation in the optimal conditions, the pre-focusing was performed during 1 min at 1500 V and the focusing during 4 min at 3000 V. The anolyte and catholyte were 0.08 M H_3PO_4 and 0.1 M NaOH (both are in 0.1 % w/w of MC solution), respectively. The pI values of the samples were determined by calibration with the 4.14 or 5.12 and 9.22 pI markers, and assuming a linear pH gradient. The icIEF cartridge was flushed with ultra-pure water and conditioning solution (4 M urea, 0.35 % w/w MC) before each measurement. 30 µL of the sample was loaded, and 17 µL was injected for each measurement. The sample tray was thermostated at a temperature of 10 °C.

2.4.3. Sample preparation

In the optimal conditions, the icIEF matrix was composed of 4 % AESlyte SH pH 3-10, 0.35 % w/w MC, 2 M urea, 0.01 % v/v Tween® 80 as well as 0.025 % w/w pI markers 4.14 or 5.12 and 9.22. 7 µL of the sample was diluted with 193 µL of the icIEF matrix to obtain a final

concentration of 35 µg mL^{-1} of HPV16-VLPs. The sample was then gently vortexed, incubated 1 h at room temperature, transferred into the sample vial, capped and placed in the autosampler for analysis.

To analyze HPV16-VLPs under reducing conditions, the icIEF matrix was composed of 4 % AESlyte SH pH 3-10, 0.35 % w/w MC, 2 M urea, 0.01 % v/v Tween® 80, 50 mM DTT, 0.025 % w/w pI markers 4.14 or 5.12 and 9.22.

To assess the method accuracy, a sample containing 0.025 % w/w pI marker 6.61 within the icIEF matrix was analyzed. Testing was conducted in triplicate across three separate days, with each sample undergoing six injections per session. The icIEF matrix was prepared freshly every day.

To evaluate the method precision, four independent samples were prepared. For repeatability, the same sample was injected six times. Two samples were analyzed on the same day, each injected three times, to assess inter-sample repeatability. Three additional samples were analyzed over three consecutive days to evaluate intermediate precision, each injected three times. The icIEF matrix was freshly prepared each day before analysis.

2.5. Bio-layer interferometry

Bio-layer interferometry (BLI) experiments were conducted as described in [23]. Briefly, LN332 (at a concentration of 1.25 µg mL^{-1}) was immobilized onto aminopropylsilane biosensors (Sartorius) for 90 s. The biosensors were then saturated using an HBSt-BSA solution buffer (10 mM HEPES-Na pH 7.6, 150 mM NaCl, 3 mM EDTA, 0.005 % v/v Tween® 20, 0.5 % w/v BSA) for 120 s to prevent non-specific binding. The association with HPV16-VLPs was recorded for 500 s using HPV16 L1 protein concentrations ranging from 16 nM to 500 nM. The dissociation was recorded in HBSt-BSA solution buffer for 500 s. Recorded data were corrected by subtracting the signals from a reference sensor immobilized with LN332 but without any analyte. We also performed control experiments with unloaded biosensors (no LN332 immobilized), the data showed no significant non-specific binding of HPV16-VLPs onto the biosensor surface. All data were analyzed using the Octet Data Analysis HT software 12.0, considering the analyte concentration as the HPV16 L1 protein concentration and fitted using the simplest binding model (1:1) and a global fit.

2.6. Affinity capillary electrophoresis

Affinity capillary electrophoresis (ACE) experiments were conducted as described in [23]. Briefly, CE analysis was conducted using a background electrolyte (BGE) consisting of 0.01 M Tris HCl, 0.01 M HEPES-Na, 0.1 M NaCl and 0.1 % w/v PEG 6000, pH 7.4 buffer containing 1.5 mM SDS, a PEO-coated capillary (48.5 cm (8.5 cm to the detector) x 50 µm), a voltage of + 10 kV, a pressure injection for 15 s at – 50 mbar, a detection at 280 nm and a cassette temperature of 15 °C. The mixture was prepared with 2.19 nM HPV16-VLPs and 26.56 nM LN332. Phthalic acid at 100 µg mL^{-1} was added to the mixtures as internal marker (M). The mixture was prepared in the following proportions: 2 µL phthalic acid solution, 8 µL HPV16-VLP solution and 10 µL LN332 solution. The HPV16-VLP standard was prepared with 10 µL PBS instead of LN332 solution.

2.7. Baculovirus genome sequencing

The quantification of the baculovirus was performed following the protocol described in [24]. Briefly, baculovirus-infected SF21 cells were extensively washed with DPBS to remove free virus particles from cells. Total cellular DNA was extracted using the High Pure PCR template Preparation kit (Roche, Bâle, Switzerland). The quantity and quality of DNA were checked using a NanoDrop ND-1000 spectrophotometer (Thermo Fisher Scientific, Waltham, USA). Next generation sequencing analysis was done by Genewiz (Leipzig, Germany).

2.8. Disassembly and reassembly

The disassembly and reassembly process was performed as previously described [25, 26]. HPV16-VLPs were incubated with 50 mM DTT at 37 °C for 20 min to induce disassembly. A portion of the sample was immediately analyzed by icIEF. The remaining volume was dialyzed overnight at 4°C using Slide-A-Lyzer™ Mini dialysis devices (2k MWCO) (Thermo Fisher Scientific, Waltham, USA) against 150 mM NaCl containing 0.01 % v/v Tween® 80 to remove excess DTT and promote reassembly.

3. Results and discussion

3.1. Development of the icIEF method

The development of the icIEF method was initiated using a matrix composed of 4 % w/w ampholytes, 0.35% w/w methylcellulose (MC) and 0.05 % w/w pI markers, loaded into a cartridge containing a fluorocarbon-coated capillary. Several parameters including surfactant addition, urea concentration and focusing time, were optimized.

3.1.1. Influence of non-ionic surfactant addition

HPV-VLPs are inherently unstable and tend to aggregate in the absence of any stabilizer. Shi et al. [27] demonstrated that the addition of a non-ionic surfactant in the sample, and more particularly Tween® 80 (polysorbate 80), helps to limit the adsorption phenomenon. Their findings indicate that Tween® 80 stabilizes HPV-VLPs not by directly interacting with them but by preventing their adsorption to surfaces. This protective effect is primarily attributed to the replacement mechanism, where Tween® 80 competes with proteins for surface adsorption, rather than the solubilization mechanism, which involves forming direct protein-surfactant complexes. It is worth noting that Tween® 80 is present in the Gardasil®9 vaccine formulation. After purification, HPV16-VLPs that we produced in the laboratory are finally resuspended in a solution of 0.15 M NaCl and 0.01 % v/v Tween® 80. To enhance analytical repeatability and minimize aggregation, the effect of varying Tween® 80 concentrations from 0.005 % v/v to 0.02 % v/v in the icIEF matrix on pI determination was evaluated. The results indicated that concentrations of 0.005 % v/v and 0.01 % v/v Tween® 80 yielded superior repeatability, with pI standard deviation (SD) values of 0.07, compared to 0.13 at 0.02 % v/v Tween® 80 (n = 6). A concentration of 0.01 % v/v Tween® 80 was selected, not only due to its stabilizing effect on the VLPs but also because it maintains consistency with the original VLP resuspension solution.

3.1.2. Optimization of urea concentration

In cIEF, urea is widely used to prevent protein aggregation and precipitation that can occur during the capillary focusing [28-30]. As a powerful solubility enhancer, urea disrupts hydrogen bond formation, reducing the risk of protein precipitation and improving the stability of the sample. Its effectiveness has made urea a popular choice for many years, especially in cIEF, where the low solubility of proteins at their pI and the use of high sample concentrations can lead to poor repeatability and the appearance of spikes [29].

The concentration of urea used must be carefully optimized, as lower amounts may be appropriate at reduced sample concentrations, while higher concentrations might be necessary to prevent aggregation in more concentrated samples. A range of urea concentrations between 1 and 6 M was investigated (Fig. 1). As shown in this figure, concentrations of 1 M and 6 M resulted in double peaks and unstable baselines. Stable profiles were observed at urea concentrations of 2 M and 4 M, with pI SD values of 0.07 and 0.08, respectively (n = 6). To preserve the integrity of the viral particles as well as to prevent cartridge damage, a lower urea concentration is preferable. As a result, a urea concentration of 2 M was selected as the optimal concentration for HPV16-VLP analysis in subsequent experiments.

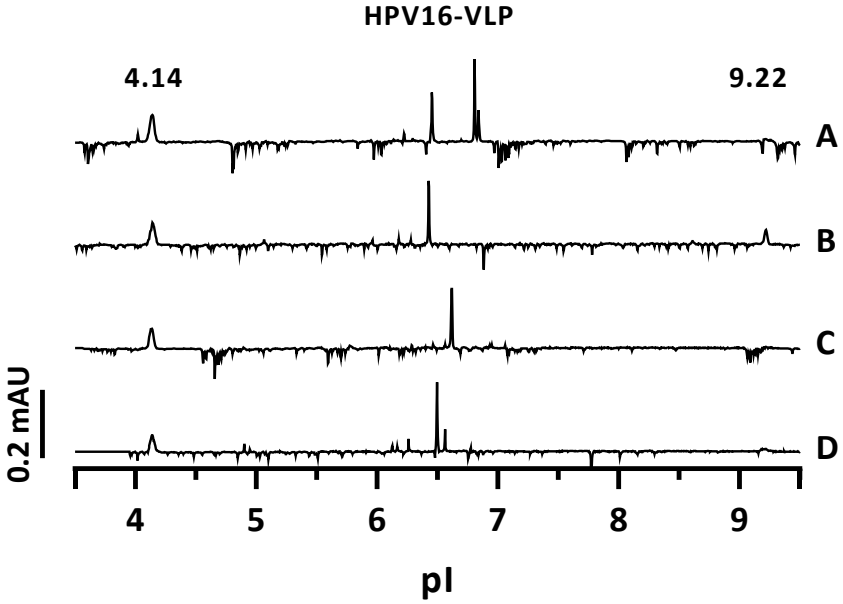

Figure 1. Influence of urea concentration in the icIEF matrix. Analysis of HPV16-VLPs with increasing urea concentrations: 1 M (A), 2 M (B), 4 M (C), and 6 M (D). The matrix composition includes 0.35 % w/w MC, 0.05 % w/w pI markers (4.14 and 9.22), 0.01 % v/v Tween® 80, and 4 % w/w AESlyte SH pH 3-10. Other conditions as described in Section 2.

277 3.1.3. Optimization of the focus time

278 The addition of urea led to an increase in the solution viscosity within the capillary and therefore
279 to a decrease in the electrophoretic mobility of the analytes. Therefore, the focusing time needs
280 to be optimized for the selected urea concentration [29, 30]. To ensure the focusing time was
281 long enough for both the pI markers and the HPV-VLPs, which have a significantly higher
282 molecular mass (i.e. 20 MDa), the focusing time was evaluated between 2 and 6 minutes. As
283 shown in Supplementary Fig. S2 trace A, a 2-minute focusing time is insufficient for HPV-VLP
284 stabilization. HPV-VLP profiles exhibited only minor variations as the focusing time was
285 varied between 3 and 6 minutes (traces B-E). Since the results of the focusing time experiments
286 were very similar, 4 minutes of focusing at 3 kV was selected to minimize the risk of
287 aggregation and reduce the analysis time.

288

289 **3.2. Method validation**

290 3.2.1. Specificity

291 The icIEF method developed for the pI determination of intact HPV16-VLPs was validated
292 following the ICH Q2(R2) guidelines [31].

293 According to those guidelines, specificity is confirmed by demonstrating that the method
294 remains unaffected by the presence of other substances, such as matrix components, and that
295 no interference with the analyte peak occurs. To verify this, an icIEF matrix sample (i.e. a blank
296 sample containing both pI markers) was prepared and analyzed to ensure that the matrix
297 components did not interfere with the analyte peak. As shown in Supplementary Fig. S3 (traces
298 A and B), there was no peak in the blank at the pI corresponding to that of HPV16-VLPs.

299 To ensure that HPV-VLP particles were still present in the sample matrix when analyzed under
300 the optimal conditions, a sample prepared in the icIEF matrix was analyzed by transmission
301 electron microscopy (TEM). As shown in Fig. 2, particles are clearly visible and their
302 morphology is intact, demonstrating that the presence of 2 M urea does not impact the viral
303 capsid.

304

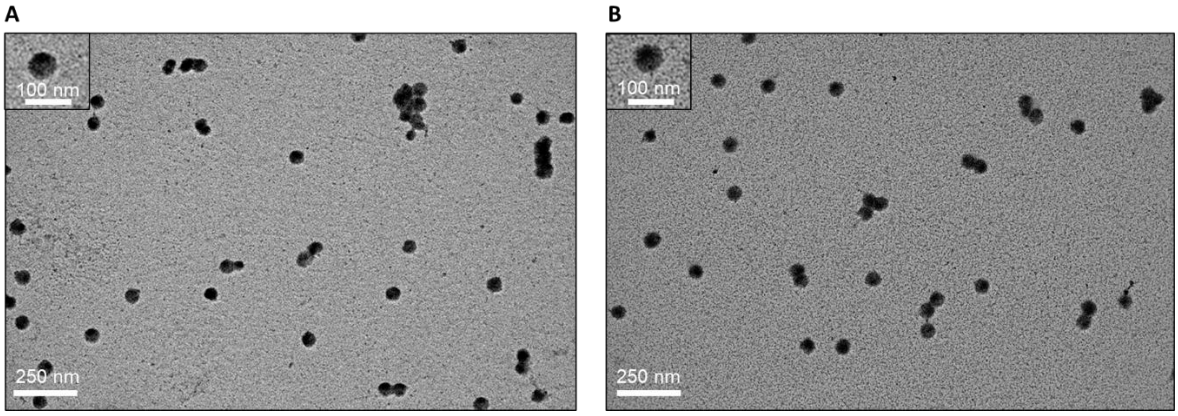

Figure 2. Ultrastructural analysis of HPV16-VLPs in the icIEF matrix (A) and in 0.15 M NaCl + 0.01 % v/v Tween® 80 (B); bars represent 250 nm. In the insert, viral particles visualized at high magnification; bars represent 100 nm.

HPV16-VLPs consist of a capsid made up of 72 pentamers (or capsomers) of L1 protein. Disulfide bonds between capsomers hold the capsid together and are important in viral assembly. The presence of disulfide bonds between capsomers enables VLP assembly to be controlled by manipulating the redox potential. Therefore, the disassembly of VLPs can be triggered by the addition of reducing agents. Moreover, it was reported that a low DTT concentration caused disassembly of VLPs into capsomers [26, 32].

To confirm that the observed peak was due to the intact particles and not to the L1 protein, a sample containing 50 mM DTT was analyzed. As illustrated in Fig. 3, the peak at a pI of 6.40 observed in the HPV16-VLP sample disappeared when DTT was added in the icIEF matrix. Instead, new peaks emerged around isoelectric points of 8.5 (framed with dotted lines in Fig. 3), possibly corresponding to the L1 monomer. The theoretical pI of the L1 monomer, calculated from its amino acid sequence using the ExPASy Compute pI/Mw tool, is 8.55, aligning with the group of peaks [33]. The multiple peaks could be attributed to L1 protein aggregation. Additionally, the sample treated with DTT was analyzed using TEM, which revealed the complete absence of particles (data not shown), providing further evidence of the dissociation of intact HPV16-VLPs in the presence of a reducing agent.

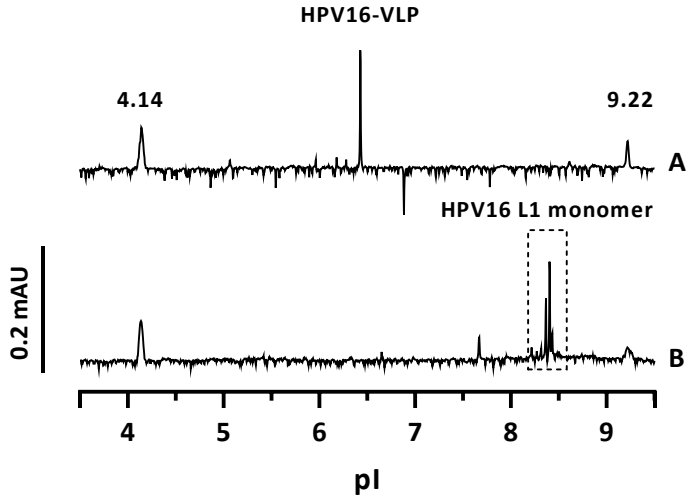

Figure 3. Analysis of HPV16-VLPs without (trace A) and with 50 mM DTT (trace B) in the icIEF matrix. The matrix composition includes 0.35 % w/w MC, 2 M urea, 0.05 % w/w pI markers (4.14 and 9.22), 0.01 % v/v Tween® 80, and 4 % w/w AESlyte SH pH 3-10. Other conditions as described in Section 2.

3.2.2 Method performance

Accurate pI determination relies on the use of pI markers with well-defined values, which are essential for assessing pI and ensuring system suitability. To validate the accuracy of pI determination, the theoretical pI value of a marker close to that of the HPV16-VLPs was compared with the experimentally obtained value. Specifically, a pI marker with a theoretical value of 6.61 was added to the icIEF matrix and the pH gradient was calibrated using pI markers at 4.14 and 9.22. Each sample was analyzed six times on three separate days. The result for the pI marker 6.61 was 6.58, with a relative bias of -0.42 %, which can be considered as very satisfactory (cf. Supplementary Fig. S3, trace C and Table 1).

For intra-sample repeatability, a single sample solution of HPV16-VLPs was prepared and analyzed in icIEF six times. For inter-sample repeatability, two sample solutions were prepared, each injected three times on the same day. Intermediate precision was evaluated by preparing three sample solutions, each injected three times over three consecutive days. The electropherograms were analyzed to estimate the pI value of HPV16-VLPs, assuming a linear correlation between pI markers of 4.14 and 9.22.

As shown in Table 1, both repeatability and intermediate precision were found to be satisfactory, with pI SD values remaining below 0.13. Although formal robustness testing was not performed, the results of the intermediate precision evaluation, obtained under slight variations in experimental conditions (such as the use of different batches of cartridges and reagents), were consistent.

Considering the obtained results, the icIEF method aiming at measuring the pI value of intact HPV16-VLPs can be considered as valid.

Table 1: Summary of validation results.

Criteria	**Parameters**	**Results**
Specificity	Absence of interference	No peak in the blank at the pI corresponding to that of HPV16-VLPs
	HPV-VLP morphology by TEM	Intact particles
	Analysis in reducing conditions	Absence of HPV16-VLP peak
Accuracy (k = 3; n = 6)	Relative bias (%) for 6.61 marker	-0.42
Intra-sample repeatability (n = 6)	pI SD	0.07
Inter-sample repeatability (2 samples; n = 3)	pI SD	0.08
Intermediate precision (k = 3; n = 3)	pI SD	0.13

3.3. Importance of pI determination for HPV16-VLP functional properties

The pI of several production batches was determined using the developed method. As shown in Fig. 4, two distinct sets of HPV16-VLPs were identified: one with a pI around 6.4 (batches 1 to 5, circled in blue), and another with a significantly higher pI (around 7.5, for batches 6 to 9 circled in orange). Notably, the latter group exhibits a shift in pI compared to the batches initially used for method development and validation. An unpaired t-test comparing the low and high pI populations confirmed that the difference is highly significant ($p < 0.001$).

To assess their suitability for use in downstream applications, these batches were subjected to the conventional QC tests, namely ELISA, electron microscopy, and SDS-PAGE. As shown in Supplementary Fig. S4, these batches successfully passed these QC tests, demonstrating the expected protein band on SDS-PAGE, acceptable antigenic reactivity in ELISA as well as the presence of particles in TEM. These results suggested that these batches meet the primary structural and antigenic requirements, despite the observed higher pI.

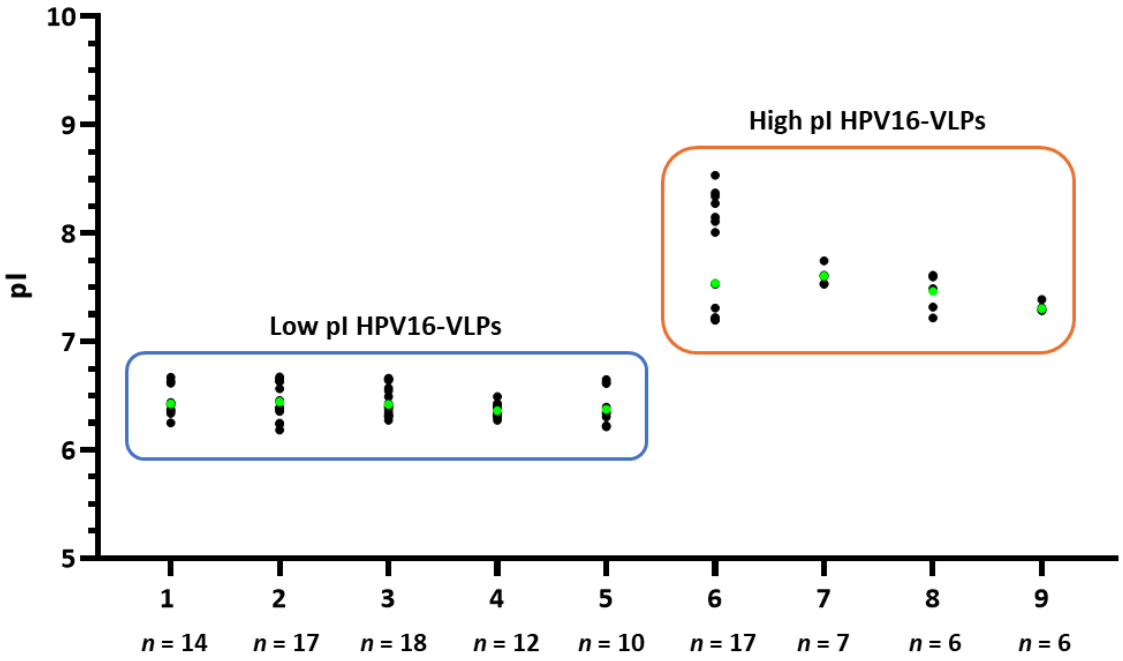

Figure 4. Isoelectric point determination of several HPV16-VLP batches. The green point represents the median pI of each batch.

To examine the functional properties of HPV16-VLPs, binding properties to host cell receptor were evaluated. HPV requires a small lesion in the skin to access and infect basal cells which are mitotically active in the lower epithelial layers. Initial binding of HPV16 is facilitated by heparan sulfate proteoglycans on keratinocytes or in the basement membrane, followed by further interactions with extracellular matrix components, and more particularly with laminin 332 (LN332) [34, 35]. These interactions may guide HPV to specific anatomical sites, but the precise receptor or binding mechanism remains under investigation, as do the binding dynamics with LN332 [2]. Very recently, the attachment properties of HPV16-VLPs to LN332 were studied by bio-layer interferometry (BLI) and affinity capillary electrophoresis (ACE) [23]. For HPV16-VLPs with a pI around 6.4, BLI analysis revealed a binding association rate (k_{on}) of 1.74×10^4 M^{-1} s^{-1} and a dissociation rate (k_{off}) of 1.50×10^{-4} s^{-1}. In ACE, a constant amount of HPV16-VLPs was preincubated with increasing LN332 concentrations, followed by the CE analysis of the mixtures. Variations in the electrophoretic mobility of the complex were followed. The K_D for the complex between HPV16-VLPs and LN332 was found to be in the nanomolar range, with values of 9 nM and 18 nM for BLI and for ACE, respectively.

When HPV16-VLPs, with a high pI, were analyzed by BLI, no association with LN332 was observed (Fig. 5 I). This result was further supported by ACE analysis, which showed no difference in electrophoretic mobility between free HPV16-VLPs and those incubated with LN332 (Fig. 5 II, traces A and B), contrary to what would be expected when the affinity is high. Together, these results highlight that HPV16-VLPs having a higher pI showed altered binding properties to LN332.

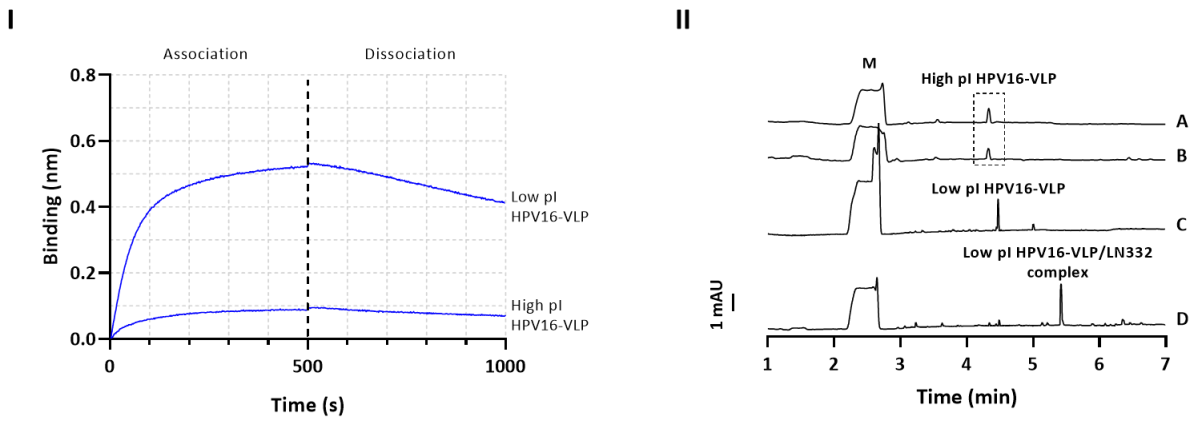

396

397 **Figure 5.** (I) Binding kinetics of high pI and low pI HPV16-VLPs to LN332 determined using BLI. Association
398 and dissociation of the complex were monitored from 0 to 500 s and from 500 to 1000 s, respectively. The HPV16
399 L1 concentration was 500 nM. (II) CE analysis of high pI HPV16-VLPs at 2.19 nM (A) and after incubation with
400 26.56 nM of LN332 (B), as well as low pI HPV16-VLPs at 2.19 nM (C) and after incubation with 26.56 nM of
401 LN332 (D). Separation conditions: BGE, 0.01 M Tris HCl, 0.01 M HEPES-Na, 0.1 M NaCl and 0.1 % w/v PEG
402 6000, pH 7.4 buffer containing 1.5 mM SDS; 48.5 cm (8.5 cm to the detector) x 50 µm PEO-coated capillary;
403 voltage + 10 kV; detection at 280 nm; pressure injection for 15 s at - 50 mbar; T = 15 °C. Other conditions as
404 described in Section 2.

405 To investigate the underlying cause of the observed difference in pI of HPV16-VLPs, the
406 possibility of structural alterations or modifications of their composition was considered.

407 One potential source of such alterations could be mutations in the baculovirus expression
408 system used for VLP production. Therefore, the baculovirus genomes used to produce the
409 batches with a high pI and those with a low pI were analyzed by next-generation sequencing in
410 order to detect any mutations that might have affected protein expression. However, the
411 comparison revealed no genetic alteration that could explain the change in pI (data not shown).

Since no genomic difference was identified, we next considered whether a conformational change in the VLPs could explain the observed pI shift. Changes in VLP conformation may alter the surface exposure of charged amino acid residues, thereby affecting their surface charge, even in the absence of sequence modifications. M. Deschuyteneer et al. [36] showed that HPV16-VLP production leads to the presence of several populations of particles, the main one having an icosahedral structure while other ones exhibit a different capsomer organization. Very recently, A. Patterson et al. [37] also showed that HPV16-VLPs exhibit significant structural heterogeneity, reflecting a complex assembly energy landscape, and a limited ability to rearrange. Moreover, it has been shown that disassembly and subsequent reassembly of VLPs results in a more homogeneous population of particles in terms of size [25, 26, 37]. To investigate whether the observed difference in pI results from conformational change, one batch of HPV16-VLPs with a high pI was subjected to a disassembly/reassembly process.

In our experiment, HPV16-VLPs, initially characterized by a high pI (Fig. 6, trace A) exhibited a shift to a low pI after disassembly/reassembly process (Fig. 6, trace C), supporting the hypothesis that a conformation change contributes to the variation in pI. As previously demonstrated, the addition of DTT leads to the formation of monomeric L1 protein (Fig. 6, trace B).

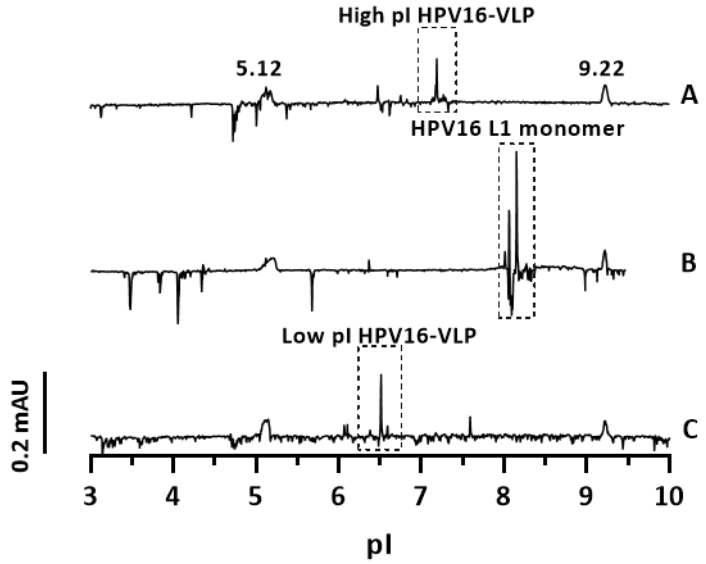

Figure 6. Analysis of HPV16-VLPs without (trace A) or with 50 mM DTT (trace B) in the icIEF matrix and the same batch of HPV16-VLPs after the disassembly/reassembly process (trace C). The matrix composition includes 0.35 % w/w MC, 2 M urea, 0.05 % w/w pI markers (5.12 and 9.22), 0.01 % v/v Tween® 80, and 4 % w/w AESlyte SH pH 3-10. Other conditions as described in Section 2.

To confirm that the reassembled HPV16-VLPs, having a low pI, retained their functional integrity, interaction studies were performed using both ACE and BLI. In ACE, a distinct electrophoretic mobility shift was observed upon complex formation (Fig. 5 II, traces C and D), indicating that the VLPs interact with their binding partner. Consistent with this, BLI analysis revealed clear association and dissociation curves at the highest VLP concentration (Fig. 5 I). The resulting binding curve yielded a K_D comparable to that of the non-reassembled material having an initial pI around 6.4 (cf. Supplementary Fig. S5), demonstrating that the reassembled particles maintain their binding affinity. These results confirm that the disassembly/reassembly process restores the functional properties of the VLPs.

HPV16-VLPs after disassembly/reassembly process were also analyzed by TEM to evaluate their integrity, size, and structural homogeneity (cf. Supplementary Fig. S6). As shown in Supplementary Fig. S7, morphological analysis by TEM showed no significant difference in the average particle diameter between HPV16-VLPs with a low pI and those with a high pI ($p > 0.05$). Moreover, both VLPs were heterogenous in size, ranging from 31 nm to 64 nm in diameter with a high pI, and from 34 nm to 65 nm with a low pI. These findings are consistent with those reported by Deschuyteneer et al. [36], who described HPV16-VLPs as having diameters ranging from 35 to 70 nm, depending on their conformation.

In a recent study, D. J. Goetschius et al performed cryo EM structural analyses of HPV16 quasivirus, composed of both capsid proteins and encapsidating a cottontail rabbit papillomavirus genome [38]. Thanks to an in-house developed software, they propose a model in which the HPV capsid exhibits dynamic behavior, continuously undergoing structural flexibility, resulting from contraction or expansion of the C-terminal arms linking the capsomers. However, the impact of this flexibility on surface charge was not evaluated. Very recently, Golushko et al. studied the influence of electrostatic interactions on viral capsids using a 2D isotropic elastic shells model [39]. They showed that transitions in the shells of *P22* bacteriophage and *Nudarelia capensis* omega virus resulted from changes in the electrostatic interactions between the capsid proteins. It would be highly interesting to apply modelling approaches to gain deeper insights into the underlying mechanisms that may explain the change in surface charge of the HPV capsid.

3.4. Control chart elaboration for batch QC

Establishing control charts for the functional characterization of HPV16-VLPs is essential to ensure the consistency and reliability of both production processes and research outcomes. By applying control limits derived from icIEF analyses across validation batches, it becomes possible to monitor batch-to-batch variability and promptly identify any deviations from defined quality standards. Based on these data, the standard deviation was calculated, and acceptance limits, corresponding to 3 SD, were defined, capturing the variation inherent to the production and allowing for the identification of deviations from the established quality standards (Fig. 7).

These control limits can then be applied in routine production to provide a statistical basis for quality assessment. By comparing these batches against the defined limits, their adherence to pre-defined quality standards was confirmed, thus ensuring process consistency. Statistical process controls, like these control charts, are crucial not only in biopharmaceutical production, where maintaining consistency in critical quality attributes is essential for regulatory compliance and ensuring product efficacy, but also to guarantee reproducibility of research data.

This tool not only helps maintain critical quality attributes during routine manufacturing but also provides a solid foundation for the reproducibility of experimental data. In the context of VLP-based vaccines or research, such controls are especially important, as variations in particle conformation or stability can directly impact immunogenicity and overall biological performance. Therefore, implementing rigorous control measures is crucial to ensure product quality, regulatory compliance, and research reproducibility.

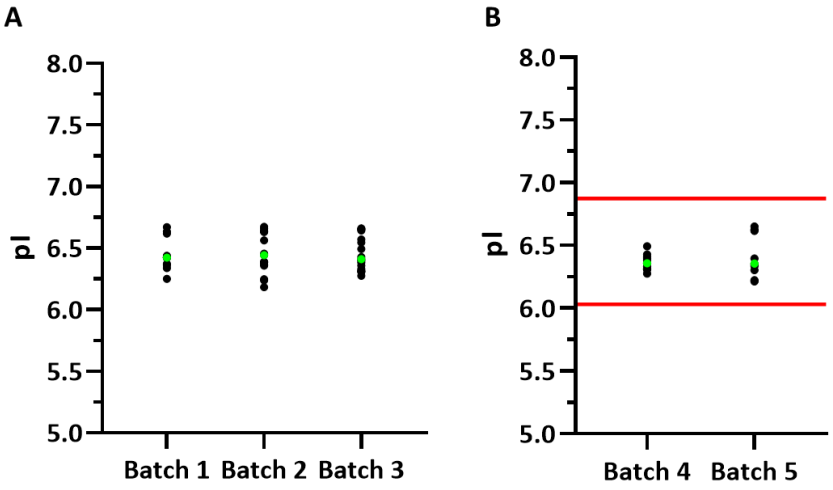

Figure 7. Establishment of a control chart based on pI determination for batch QC. Results for the 3 validation batches (A) and control chart of routine batches (B). Red lines represent the acceptance limits, and the green or red point represents the median pI of each batch.

4. Concluding remarks

This work demonstrates that icIEF is a valuable analytical tool for assessing the structural integrity and batch consistency of HPV16-VLPs. The optimized and validated method allowed the identification of subtle conformational differences between VLP batches that were undetectable by conventional QC methods. Importantly, these differences correlated with variations in binding affinity to the physiological receptor LN332, underlining their potential impact on biological function. Furthermore, the successful restoration of both pI and binding properties following disassembly/reassembly process indicates that conformational change is probably the key driver. If the measured pI of HPV16-VLP batches falls outside the acceptance limits, applying such a protocol can be considered to recover the intended structural and functional properties. Stability studies of HPV16-VLP batches using the validated icIEF method could be performed in order to assess their quality over time.

By enabling sensitive detection of such differences, the icIEF method provides a powerful means to evaluate the reproducibility and quality of VLP-based products. The implementation of this method into routine quality control strategies could enhance both the reliability of research outcomes and the safety and efficacy of VLP-based vaccines. Importantly, while this study focused on HPV16-VLPs, these particles share common structural features with other types of VLPs used as research models, in vaccines and in immunotherapy, such as those developed to treat peanut allergy [40]. Since they result from the self-assembly of capsid protein(s), they display multiple native epitopes on their surface. This highlights the potential of icIEF as a platform-wide tool for the rapid QC of diverse VLP research models and vaccine candidates.

Acknowledgements

Many thanks are due to “Fonds spéciaux à la recherche” of the University of Liège and Fonds Leon Fredericq for their financial support. The authors are grateful to Pr. Antoine Touzé (UMR INRAE ISP, Université de Tours, Tours, France) for the provision of SF21 cells. They also thank Pr. Martin Müller (German Cancer Research Center, Heidelberg, Germany) for providing the baculovirus expressing HPV16 L1 and HPV16 L1 conformational antibody supernatant. Finally, the authors acknowledge Pr. André Matagne and the Robotein platform of the BE Instruct-ERIC Centre for providing access to the Octet HTX.

References

[1] H. Sung *et al.*, "Global Cancer Statistics 2020: GLOBOCAN Estimates of Incidence and Mortality Worldwide for 36 Cancers in 185 Countries," *CA Cancer J Clin*, vol. 71, no. 3, pp. 209–249, 2021, doi: 10.3322/caac.21660.

[2] A. A. McBride, "Human papillomaviruses: diversity, infection and host interactions," *Nat Rev Microbiol*, vol. 20, no. 2, pp. 95–108, 2022, doi: 10.1038/s41579-021-00617-5.

[3] S. de Sanjosé, M. Brotons, and M. A. Pavón, "The natural history of human papillomavirus infection," *Best Pract Res Clin Obstet Gynaecol*, vol. 47, pp. 2–13, 2018, doi: 10.1016/j.bpobgyn.2017.08.015.

[4] L. S. A. Mühr, C. Eklund, and J. Dillner, "Towards quality and order in human papillomavirus research," *Virology*, vol. 519, pp. 74–76, 2018, doi: 10.1016/j.virol.2018.04.003.

[5] E. M. Burd, "Human Papillomavirus and Cervical Cancer," *Clin Microbiol Rev*, vol. 16, no. 1, pp. 1–17, 2003, doi: 10.1128/cmr.16.1.1-17.2003.

[6] C. B. Buck, C. D. Thompson, Y.-Y. S. Pang, D. R. Lowy, and J. T. Schiller, "Maturation of Papillomavirus Capsids," *J Virol*, vol. 79, no. 5, pp. 2839–2846, 2005, doi: 10.1128/jvi.79.5.2839-2846.2005.

[7] C. B. Buck *et al.*, "Arrangement of L2 within the Papillomavirus Capsid," *J Virol*, vol. 82, no. 11, pp. 5190–5197, 2008, doi: 10.1128/jvi.02726-07.

[8] J. W. Wang and R. B. S. Roden, "L2, the minor capsid protein of papillomavirus," *Virology*, vol. 445, no. 1–2, pp. 175–186, 2013, doi: 10.1016/j.virol.2013.04.017.

[9] J. Chen *et al.*, "Critical Residues Involved in the Coassembly of L1 and L2 Capsid Proteins of Human Papillomavirus 16," *J Virol*, vol. 97, no. 3, 2023, doi: 10.1128/jvi.01819-22.

[10] P. Le Cann, P. Coursaget, S. Iochmann, and A. Touze, "Self-assembly of human papillomavirus type 16 capsids by expression of the L1 protein in insect cells," *FEMS Microbiol Lett*, vol. 117, no. 3, pp. 269–274, 1994, doi: 10.1111/j.1574-6968.1994.tb06778.x.

[11] B. Raynal, P. Lenormand, B. Baron, S. Hoos, and P. England, "Quality assessment and optimization of purified protein samples: why and how?," *Microb Cell Fact*, vol. 13, pp. 1–10, 2014, doi: 10.1186/s12934-014-0180-6.

[12] N. Berrow *et al.*, "Quality control of purified proteins to improve data quality and reproducibility: results from a large-scale survey," *European Biophysics Journal*, vol. 50, no. 3–4, pp. 453–460, 2021, doi: 10.1007/s00249-021-01528-2.

[13] A. Zeltins, "Construction and Characterization of Virus-Like Particles: a Review," *Mol Biotechnol*, vol. 53, no. 1, pp. 92–107, 2013, doi: 10.1007/s12033-012-9598-4.

[14] J. Wu, W. McElroy, J. Pawliszyn, and C. D. Heger, "Imaged capillary isoelectric focusing: Applications in the pharmaceutical industry and recent innovations of the technology," *TrAC Trends in Analytical Chemistry*, vol. 150, p. 116567, 2022, doi: 10.1016/j.trac.2022.116567.

[15] J. Kahle and H. Wätzig, "Determination of protein charge variants with (imaged) capillary isoelectric focusing and capillary zone electrophoresis," *Electrophoresis*, vol. 39, no. 20, pp. 2492–2511, 2018, doi: 10.1002/elps.201800079.

[16] C. M. Zhou, "Characterization of human papillomavirus by capillary isoelectric focusing with whole-column imaging detection," *Electrophoresis*, vol. 34, no. 20–21, pp. 3046–3053, 2013, doi: 10.1002/elps.201300161.

[17] J. Du *et al.*, "Finger printing human norovirus-like particles by capillary isoelectric focusing with whole column imaging detection," *Virus Res*, vol. 311, p. 198700, 2022, doi: 10.1016/j.virusres.2022.198700.

[18] L. Goodridge, C. Goodridge, J. Wu, M. Griffiths, and J. Pawliszyn, "Isoelectric Point Determination of Norovirus Virus-like Particles by Capillary Isoelectric Focusing with Whole Column Imaging Detection," *Anal Chem*, vol. 76, no. 1, pp. 48–52, 2004, doi: 10.1021/ac034848S.

[19] X. Zhang *et al.*, "Robust manufacturing and comprehensive characterization of recombinant hepatitis E virus-like particles in Hecolin®," *Vaccine*, vol. 32, no. 32, pp. 4039–4050, 2014, doi: 10.1016/j.vaccine.2014.05.064.

[20] Z. Liu and J. Pawliszyn, "Behaviors of the MS2 virus and related antibodies in capillary isoelectric focusing with whole-column imaging detection," *Electrophoresis*, vol. 26, no. 3, pp. 556–562, 2005, doi: 10.1002/elps.200410075.

[21] Y. E. Thomassen, G. Van Eikenhorst, L. A. Van Der Pol, and W. A. M. Bakker, "Isoelectric point determination of live polioviruses by capillary isoelectric focusing with whole column imaging detection," *Anal Chem*, vol. 85, no. 12, pp. 6089–6094, 2013, doi: 10.1021/ac400968q.

[22] V. Bettonville *et al.*, "Study of intact virus-like particles of human papillomavirus by capillary electrophoresis," *Electrophoresis*, vol. 37, no. 4, pp. 579–586, Feb. 2016, doi: 10.1002/elps.201500431.

[23] A. Boclinville *et al.*, "Interaction studies between human papillomavirus virus-like particles and laminin 332 by affinity capillary electrophoresis assisted by bio-layer interferometry," *Talanta*, vol. 270, p. 125602, 2024, doi: 10.1016/j.talanta.2023.125602.

[24] N. G. Naik, Y. W. Lo, T. Y. Wu, C. C. Lin, S. C. Kuo, and Y. C. Chao, "Baculovirus as an efficient vector for gene delivery into mosquitoes," *Sci Rep*, vol. 8, no. 1, p. 17778, 2018, doi: 10.1038/s41598-018-35463-8.

[25] H. Mach *et al.*, "Disassembly and Reassembly of Yeast-Derived Recombinant Human Papillomavirus Virus-like Particles (HPV VLPs)," *J Pharm Sci*, vol. 95, no. 10, pp. 2195–2206, 2006, doi: 10.1002/jps.20696.

[26] M. P. Mccarthy, W. I. White, F. Palmer-Hill, S. Koenig, and J. A. Suzich, "Quantitative Disassembly and Reassembly of Human Papillomavirus Type 11 Viruslike Particles In Vitro," *J Virol*, vol. 72, no. 1, pp. 32–41, 1998, doi: 10.1128/jvi.72.1.32-41.1998.

[27] L. Shi *et al.*, "Stabilization of Human Papillomavirus Virus-like Particles by Non-Ionic Surfactants," *J Pharm Sci*, vol. 94, no. 7, pp. 1538–1551, 2005, doi: 10.1002/jps.20377.

[28] X. Zhang, S. Voronov, N. Mussa, and Z. Li, "A novel reagent significantly improved assay robustness in imaged capillary isoelectric focusing," *Anal Biochem*, vol. 521, pp. 1–7, 2017, doi: 10.1016/j.ab.2016.12.013.

[29] X. Z. He, A. H. Que, and J. J. Mo, "Analysis of charge heterogeneities in mAbs using imaged CE," *Electrophoresis*, vol. 30, no. 5, pp. 714–722, 2009, doi: 10.1002/elps.200800636.

[30] M. Conti, M. Galassi, A. Bossi, and P. G. Righetti, "Capillary isoelectric focusing: the problem of protein solubility," *J Chromatogr A*, vol. 757, pp. 237–245, 1997, doi: 10.1016/S0021-9673(96)00666-8.

[31] "ICH Q2(R2). Validation of analytical procedures. Final Version Adopted on 14 June 2024.".

[32] M. Sapp, C. Volpers, M. Müller, and R. E. Streeck, "Organization of the major and minor capsid proteins in human papillomavirus type 33 virus-like particles," *Journal of General Virology*, vol. 76, pp. 2407–2412, 1995, doi: 10.1099/0022-1317-76-9-2407.

[33] "Swiss Institute of Bioinformatics. ExPASy (Bioinformatics Resource Tool): Compute pI/Mw Tool (https://web.expasy.org/compute_pi/)."

[34] T. R. Broutian, S. A. Brendle, and N. D. Christensen, "Differential binding patterns to host cells associated with particles of several human alphapapillomavirus types," *Journal of General Virology*, vol. 91, pp. 531–540, 2010, doi: 10.1099/vir.0.012732-0.

[35] H.-C. Selinka *et al.*, "Inhibition of Transfer to Secondary Receptors by Heparan Sulfate-Binding Drug or Antibody Induces Noninfectious Uptake of Human Papillomavirus," *J Virol*, vol. 81, no. 20, pp. 10970–10980, 2007, doi: 10.1128/jvi.00998-07.

[36] M. Deschuyteneer *et al.*, "Molecular and structural characterization of the L1 virus-like particles that are used as vaccine antigens in Cervarix™, the AS04-adjuvanted HPV-16 and -18 cervical cancer vaccine," *Hum Vaccin*, vol. 6, no. 5, pp. 407–419, 2010, doi: 10.4161/hv.6.5.11023.

[37] A. Patterson *et al.*, “Heterogeneity of HPV16 virus-like particles indicates a complex assembly energy surface,” *Virology*, vol. 600, p. 110211, 2024, doi: 10.1016/j.virol.2024.110211.
[38] D. J. Goetschius, S. R. Hartmann, S. Subramanian, C. M. Bator, N. D. Christensen, and S. L. Hafenstein, “High resolution cryo EM analysis of HPV16 identifies minor structural protein L2 and describes capsid flexibility,” *Sci Rep*, vol. 11, 2021, doi: 10.1038/s41598-021-83076-5.
[39] I. Y. Golushko, D. S. Roshal, O. V. Konevtsova, S. B. Rochal, and R. Podgornik, “Electrostatic interactions and structural transformations in viral shells,” *Nanoscale*, vol. 16, no. 43, pp. 20182–20193, 2024, doi: 10.1039/d4nr02612h.
[40] J. M. Sobczak *et al.*, “The next generation virus-like particle platform for the treatment of peanut allergy,” *Allergy: European Journal of Allergy and Clinical Immunology*, vol. 78, no. 7, pp. 1980–1996, 2023, doi: 10.1111/all.15704.